

# Near-Perfect Single-Photon Source via Ultrastrong Coupling

Ying Ren,<sup>1</sup> Ying-Xue Ma,<sup>1</sup> and Jin-Feng Huang<sup>1,2,3,\*</sup>

<sup>1</sup>*Key Laboratory of Low-Dimensional Quantum Structures and Quantum Control of Ministry of Education, Key Laboratory for Matter Microstructure and Function of Hunan Province, Department of Physics and Synergetic Innovation Center for Quantum Effects and Applications, Hunan Normal University, Changsha 410081, China*

<sup>2</sup>*Institute of Interdisciplinary Studies, Hunan Normal University, Changsha 410081, China*

<sup>3</sup>*Hunan Research Center of the Basic Discipline for Quantum Effects and Quantum Technologies, Hunan Normal University, Changsha 410081, China*

(Dated: July 2, 2026)

Deterministic single-photon sources are indispensable core devices for quantum information technology, yet high-performance implementation remains a long-standing bottleneck for linear optical quantum computing. We propose a feasible scheme for deterministic single-photon emission based on a  $\Delta$ -type three-level atom coupled to a single-mode cavity, driven by two classical external fields, which is adaptable to both strong and ultrastrong cavity-atom coupling regimes. Under continuous-wave driving, the system achieves excellent single-photon characteristics: the normalized equal-time second-order correlation function reaches  $g^{(2)}(0) \sim 10^{-6}$ , with a photon indistinguishability of 98.73% and a state purity of 99.95% in the strong coupling regime, while the ultrastrong coupling regime further suppresses  $G^{(2)}(0) \sim 10^{-8}$ , yielding an indistinguishability of 99.10% and a purity of 99.99%. For pulsed driving in the ultrastrong coupling regime, the source realizes superior performance, with an emission efficiency, indistinguishability, and purity of 99.96%, 98.98%, and 99.99% under resonant conditions, and 100%, 95.91%, and 99.93% under detuned conditions, respectively. The near-ideal optical performance of the proposed scheme provides a viable route for constructing high-quality deterministic single-photon sources, which offers a promising solution to the limitations of conventional single-photon devices and facilitates the further development of quantum information science and fundamental quantum optical research.

## I. INTRODUCTION

Single-photon sources are crucial for quantum information science [1], ultrasensitive quantum sensing and metrology [2, 3], quantum technologies [4], and fundamental quantum physics [5]. In particular, they serve as key hardware for quantum communication [5–8], photonic quantum computing [9–12], and quantum networks [13, 14]. An ideal single-photon source is capable of deterministically emitting one photon per excitation, and is expected to simultaneously exhibit near-unity purity ( $g^{(2)}(0) \rightarrow 0$ ), high photon indistinguishability ( $I \rightarrow 1$ ), unit efficiency, scalability, and other favorable performances. Nevertheless, realizing a source that satisfies all these requirements remains a formidable challenge, and trade-offs among these figures of merit are generally unavoidable. A low second-order correlation  $g^{(2)}(0) < 0.01$  is difficult to attain due to multiphoton emission and environmental noise. Photon indistinguishability is easily degraded by spectral broadening of emitted photons and coupling fluctuations in circuit cavity quantum electrodynamics. Additionally, the overall efficiency is restricted by mode mismatch between emitters such as quantum dots and nitrogen-vacancy (NV) centers and optical cavities, interfacial losses, as well as the intrinsic limits imposed by the cavity quality factor  $Q$  and mode volume  $V$ .

Single-photon sources based on individual quantum emitters such as atoms [15, 16], molecules [17], ions [18], NV centers [19], 2D materials [20], quantum dots [21, 22] and cavity QED systems [23] have been realized experimentally. Semiconductor quantum dots are currently the most mature platform, but they are restricted by fixed emission wavelengths and limited array scalability. A recent experiment on a microcavity-coupled quantum dot at 4 K reports a system efficiency of 71.2%, photon indistinguishability of 98.6% and single-photon purity over 98% [10]. Nevertheless, high-performance single-photon sources are still highly desirable for theoretical and experimental research [24].

We put forward a practical scheme to generate single photons deterministically. We study a  $\Delta$ -type three-level atom [25–29] confined in a high-finesse cavity. Its two excited levels couple to a single cavity mode to form the Jaynes-Cummings (JC) model [30–33]. Two classical fields resonantly drive the transitions from the ground state to the two excited states. Under resonant driving, the system reduces to an effective  $\Lambda$ -type three-level system. A Raman transition via the lowest single-excitation eigenstate of the JC model gives rise to single-photon emission. For large detuning, the  $\Lambda$  system can be further simplified into a two-level system for deterministic photon generation. We explore continuous-wave and pulsed driving for strong and ultrastrong coupling regimes. For resonant continuous-wave driving in the strong coupling regime, we achieve  $g^{(2)}(0) \sim 10^{-6}$ , 98.73% indistinguishability and 99.95% purity. In the ultrastrong coupling regime,  $G^{(2)}(0) \sim 10^{-8}$ , with indis-

\* Contact author: [jfhuang@hunnu.edu.cn](mailto:jfhuang@hunnu.edu.cn)

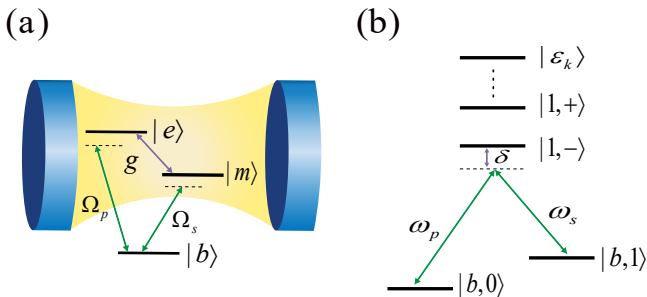


FIG. 1. (Color online) (a) Schematic of the system. A  $\Delta$ -type three-level atom interacts with the cavity mode via its two excited states  $|e\rangle$  and  $|m\rangle$ . The transitions  $|m\rangle \leftrightarrow |b\rangle$  and  $|e\rangle \leftrightarrow |b\rangle$  are driven by two external fields with frequencies  $\omega_p$  and  $\omega_s$ , respectively. The excited states  $|e\rangle$  and  $|m\rangle$  are resonantly coupled to a single cavity mode. (b) Energy-level diagram of the effective  $\Lambda$  system. The initial state  $|b,0\rangle$  and final state  $|b,1\rangle$  are connected by the driving field through the eigenstates  $|\varepsilon_k\rangle$  of the Jaynes-Cummings model. The detuning  $\delta$  is defined as the difference between the driving frequency  $\omega_p$  ( $\omega_s$ ) and the transition frequency from  $|b,0\rangle$  ( $|b,1\rangle$ ) to  $|\varepsilon_k\rangle$ .

tinguishability of 99.10% and purity of 99.99%. Pulsed driving also delivers outstanding performance: in the ultrastrong coupling regime, the efficiency, indistinguishability and purity reach 99.96%, 98.98% and 100% at resonance, and 100%, 95.91% and 99.93% off resonance. All metrics meet the criteria of linear optical quantum computing without performance trade-offs, demonstrating near-ideal single-photon emission. Our scheme supports wavelength tuning via cavity mode frequency and works across a broad parameter space, fully compatible with current experimental capabilities. It can effectively overcome the wavelength limitation of quantum dot systems.

The rest of this paper is organized as follows. Section II presents the physical model and Hamiltonian, and analyzes the system dynamics under resonant and detuned conditions. Section III investigates the system performance with dissipative effects and compares the performance of different driving strategies in the strong coupling regime. Section IV further explores the dissipative system performance and conducts a comparative analysis of diverse driving schemes in the ultrastrong coupling regime. Conclusions and experimental outlook are given in Section V.

## II. MODEL AND HAMILTONIAN

We consider a  $\Delta$ -type three-level atomic system, where the two excited energy levels  $|e\rangle$  and  $|m\rangle$  are resonantly coupled to a single-mode cavity field with resonant frequency  $\omega_c$ . The energy spacing between the intermediate level  $|m\rangle$  and the ground level  $|b\rangle$  is set to be much larger than the cavity frequency  $\omega_c$ , such that the atom

residing in the ground state  $|b\rangle$  does not couple to the cavity field. The system is initially prepared in the state  $|\psi(0)\rangle = |b,0\rangle$ , corresponding to the atom in the ground state  $|b\rangle$  and the cavity in the vacuum state. To achieve deterministic single-photon emission, two external classical driving fields with frequencies  $\omega_s$  and  $\omega_p$  are applied to drive the atomic transitions  $|e\rangle \leftrightarrow |b\rangle$  and  $|m\rangle \leftrightarrow |b\rangle$ , respectively, as schematically illustrated in Fig. 1(a). The total Hamiltonian of the system reads

$$H = H_0 + H_1, \quad (1)$$

where  $H_0$  represents the part without driving fields ( $\hbar = 1$ ):

$$H_0 = \omega_c a^\dagger a + \omega_e |e\rangle\langle e| + \omega_m |m\rangle\langle m| + \omega_b |b\rangle\langle b| + g(|e\rangle\langle m|a + a^\dagger|m\rangle\langle e|), \quad (2)$$

and  $H_1$  describes the interaction part with the two external driving fields:

$$H_1 = \Omega_p \cos(\omega_p t)(|e\rangle\langle b| + |b\rangle\langle e|) + \Omega_s \cos(\omega_s t)(|m\rangle\langle b| + |b\rangle\langle m|). \quad (3)$$

Here,  $a(a^\dagger)$  is the annihilation (creation) operator of the cavity field,  $\omega_i$  ( $i = e, m, b$ ) is atomic frequency of the atomic level  $|i\rangle$ ,  $g$  is the atom-cavity coupling strength, and  $\Omega_p$  and  $\Omega_s$  are the Rabi frequencies of the two external driving fields.

Note that  $H_{JC} = \omega_c a^\dagger a(|e\rangle\langle e| + |m\rangle\langle m|) + \omega_e |e\rangle\langle e| + \omega_m |m\rangle\langle m| + g(|e\rangle\langle m|a + a^\dagger|m\rangle\langle e|)$  describing the JC model [30], in terms of the eigenstates  $|\varepsilon_k\rangle$  of  $H_{JC}$  satisfying  $H_{JC}|\varepsilon_k\rangle = \varepsilon_k|\varepsilon_k\rangle$ , we can rewrite  $H_0 = H_{JC} + \omega_c a^\dagger a|b\rangle\langle b| + \omega_b |b\rangle\langle b|$ , as diagonal form:

$$H_0 = \sum_{k=0}^{\infty} \varepsilon_k |\varepsilon_k\rangle\langle \varepsilon_k| + \sum_{n=0}^{\infty} (\omega_b + n\omega_c) |b, n\rangle\langle b, n|. \quad (4)$$

The states  $|\varepsilon_k\rangle$  are defined as  $|\varepsilon_0\rangle \equiv |m, 0\rangle$ ,  $|\varepsilon_{2n-1}\rangle \equiv |n, -\rangle = -\sin\theta_n |e, n-1\rangle + \cos\theta_n |m, n\rangle$ , and  $|\varepsilon_{2n}\rangle \equiv |n, +\rangle = \cos\theta_n |e, n-1\rangle + \sin\theta_n |m, n\rangle$  ( $n = 1, 2, \dots$ ). Here, the subscript  $n$  label the  $n$  excitation subspace of the JC Hamiltonian and the angle  $\theta_n$  are defined by  $\cos\theta_n = (2g\sqrt{n}) / [(\tilde{\Omega}_n - \Delta)^2 + 4g^2n]^{1/2}$ , where  $\tilde{\Omega}_n = \sqrt{\Delta^2 + 4g^2n}$  is the generalized Rabi frequency and  $\Delta = \omega_e - \omega_m - \omega_c$  is the detuning from the cavity field of the level space between  $|e\rangle$  and  $|m\rangle$ . Meanwhile, we define the probability amplitudes as  $c_{kn} = \langle \varepsilon_k | m, n \rangle$  and  $d_{kn} = \langle \varepsilon_k | e, n \rangle$ . Similarly, the driving Hamiltonian  $H_1$  can be rewritten as:

$$H_1 = \sum_{n,k=0}^{\infty} \lambda_{kn}(t) (|b, n\rangle\langle \varepsilon_k| + \varepsilon_k\langle b, n|), \quad (5)$$

where  $\lambda_{kn}(t) \equiv \Omega_p d_{kn} \cos(\omega_p t) + \Omega_s c_{kn} \cos(\omega_s t)$  is introduced.

$H_1$  describes many transition processes, where certain resonant transitions can be selected by tuning the driving

field frequencies  $\omega_p$  and  $\omega_s$ . We focus on the Raman resonant condition

$$\omega_p - \omega_s = \omega_c, \quad (6)$$

which enables resonant transitions from the initial state  $|b, 0\rangle$  to the target state  $|b, 1\rangle$  via intermediate state  $|1, -\rangle$  and some higher-energy levels through the Raman transition, as shown in Fig. 1(b). When the driving fields is sufficiently weak, the resonant coupling is dominant and only the states involved in the resonant coupling can be effectively accessed.

In the interaction picture defined by  $U(t) = \exp(-iH_0t)$ , the system Hamiltonian  $H$  becomes

$$H_I = \sum_{n,k=0}^{\infty} \sum_{q=\pm 1} (\chi_{p,kn} e^{i\delta_{kn,qp}t} + \chi_{s,kn} e^{i\delta_{kn,qs}t}) |\varepsilon_k\rangle \langle b, n| + \text{H.c.}, \quad (7)$$

where  $\chi_{p,kn}$ ,  $\chi_{s,kn}$  and the detuning  $\delta_{kn,ql}$  ( $l = p, s$ ) are defined as

$$\begin{aligned} \chi_{p,kn} &= \frac{\Omega_p}{2} d_{kn}, \\ \chi_{s,kn} &= \frac{\Omega_s}{2} c_{kn}, \\ \delta_{kn,ql} &= \varepsilon_k - \omega_b - n\omega_c + q\omega_l, \quad (q = \pm 1). \end{aligned} \quad (8)$$

The effective coupling strength  $\chi_{p,kn}$  and  $\chi_{s,kn}$  are dependent on the coefficient  $d_{kn}$  and  $c_{kn}$ . When the cavity field resonantly couple to with the upper two levels  $|e\rangle$  and  $|m\rangle$ , namely  $\Delta = 0$ ,  $d_{kn}$  and  $c_{kn}$  become constants. As we shall discuss in the following  $H_I$  can be well approximated by keeping only  $n = 0$  and  $n = 1$  terms.

### A. Large detuning case

We first consider the large detuning case defined by the conditions:  $\delta \equiv \varepsilon_1 - \omega_b - \omega_p \gg (\Omega_p \cos \theta_1/2)$  and  $\varepsilon_1 - \omega_b - \omega_c - \omega_s \gg (\Omega_s \sin \theta_1/2)$  under which the energy levels  $|\varepsilon_k\rangle$  ( $k = 0, 1, 2, \dots$ ) can be adiabatically eliminates. Using the time-averaging method [34, 35] with Raman resonance condition (6), we can adiabatically eliminate the energy levels  $|\varepsilon_k\rangle$  ( $k = 0, 1, 2, \dots$ ), then the Hamiltonian  $H_I$  becomes:

$$H'_{eff} \cong \sum_{n=0}^{\infty} \Delta_n |b, n\rangle \langle b, n| + \sum_{n=0}^{\infty} g_{n,n+1} |b, n\rangle \langle b, n+1| + \text{H.c.} \quad (9)$$

Here the ac Stark shifts  $\Delta_n$  and effective coupling strength  $g_{n,n+1}$  are defined as

$$\Delta_n = - \sum_{k=0}^{\infty} \sum_{l=s,p} \sum_{q=\pm 1} \frac{|\chi_{kn,l}|^2}{\delta_{kn,ql}}, \quad (10)$$

$$g_{n,n+1} = - \sum_{k=0}^{\infty} \frac{(\Omega_s c_{kn+1})(\Omega_p d_{kn})^*}{4\delta_{kn,-1p}}. \quad (11)$$

During the derivation of Eq. (9), we have discard the rapidly oscillating terms, such as higher-order transition terms of the form  $|b, n+m\rangle \langle b, n|$  ( $m \geq 2$ ). This approximation is valid due to the detuning difference in the multiphoton process  $|b, n\rangle \rightarrow |\varepsilon_k\rangle \rightarrow |b, n+m\rangle$  with  $m \geq 2$ , is significantly larger than that in the single-photon Raman process  $|b, n\rangle \rightarrow |\varepsilon_k\rangle \rightarrow |b, n+1\rangle$ .

Under the condition of weak driving with  $\Omega_p/\omega_c < 0.01$ , we find that  $g_{1,2} \ll g_{0,1}$ . With the condition  $g_{1,2}t \ll 1$ , the transition from  $|b, 1\rangle$  to  $|b, 2\rangle$  can be ignored. Eq. (9) is therefore further simplified, enabling a valid truncate and yielding the effective Hamiltonian

$$H''_{eff} = \Delta_0 |b, 0\rangle \langle b, 0| + \Delta_1 |b, 1\rangle \langle b, 1| + g_{0,1} |b, 0\rangle \langle b, 1| + \text{H.c.} \quad (12)$$

Thus, the system simplifies to an effective two-level system, where coherent Rabi oscillations take place between the states  $|b, 0\rangle$  and  $|b, 1\rangle$ . Specifically, when the detuning satisfies  $\Delta_0 = \Delta_1$ , at time  $t = \pi/(2g_{0,1})$ , the state  $|b, 0\rangle$  is completely transferred to the state  $|b, 1\rangle$ , generating a single photon due to  $|b\rangle$  dose not couple to the cavity. The single cavity photon is free as a real photon, when the driving field is switched off at time  $t = \pi/(2g_{0,1})$ . Physically, the creation of the single photon is due to the intermediate state  $|1, -\rangle$  where  $\sin \theta_1 |m, 1\rangle$  provides the transition matrix element.

We note that the condition  $\Delta_0 = \Delta_1$  corresponds to the balanced state of ac Stark shifts. This condition can be achieved by precisely tuning the intensity ratio of the driving fields at the ratio

$$\alpha \equiv \frac{\Omega_s}{\Omega_p} = \sqrt{\frac{f(d_{k0}, d_{k1}, \omega_p)}{f(c_{k0}, c_{k1}, \omega_s)}} \quad (13)$$

where

$$f(x, y, z) = \sum_{k=0}^{\infty} \frac{|x|^2 (\varepsilon_k - \omega_b)}{(\varepsilon_k - \omega_b)^2 - z^2} - \sum_{k=0}^{\infty} \frac{|y|^2 (\varepsilon_k - \omega_b - \omega_c)}{(\varepsilon_k - \omega_b - \omega_c)^2 - z^2}. \quad (14)$$

### B. Resonant case

Now we consider the resonant case: the pump field resonantly drives the transition  $|b, 0\rangle \leftrightarrow |1, -\rangle$ , i.e.,  $\delta = 0$ ; and the Stokes driving fields resonantly drives the transition  $|1, -\rangle \leftrightarrow |b, 1\rangle$ , i.e.,  $\varepsilon_1 - \omega_b - \omega_c - \omega_s = 0$ . Under these conditions, all the other eigenstates  $|\varepsilon_k\rangle$  ( $k \neq 1$ ) are far off resonance and can be discarded. Then Eq. (7) can be reduce to an effective  $\Lambda$ -type three-level Hamiltonian:

$$H_{eff} = \chi_p |\varepsilon_1\rangle \langle b, 0| + \chi_s |\varepsilon_1\rangle \langle b, 1| + \text{H.c.}, \quad (15)$$

where  $\chi_p = -(\sqrt{2}\Omega_p)/4$  and  $\chi_s = (\sqrt{2}\Omega_s)/4$ .

By solving the Schrödinger equation with the effective Hamiltonian (15), we derive the single-photon transition

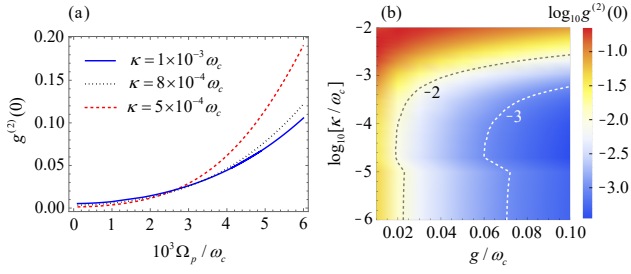


FIG. 2. (Color online) (a) Equal-time second-order correlation function  $g^{(2)}(0)$  as a function of the driving amplitude  $\Omega_p$  on resonance ( $\delta = 0$ ) with  $g = 0.05\omega_c$  and  $\kappa_i = \kappa = 10^{-3}\omega_c$  [ $i = 1, 2, 3$ , blue solid curve],  $8 \times 10^{-4}\omega_c$  (black dotted curve), and  $5 \times 10^{-4}\omega_c$  (red dashed curve), respectively. (b)  $g^{(2)}(0)$  as functions of the coupling strength  $g$  and the damping rate  $\kappa_i = \kappa$  ( $i = 1, 2, 3$ ) on resonance ( $\delta = 0$ ) for  $\Omega_p = 10^{-3}\omega_c$ . The black and white dashed curves label  $g^{(2)}(0) = 10^{-2}$  and  $g^{(2)}(0) = 10^{-3}$ , respectively. Other common parameters are:  $\Omega_s = \alpha_c\Omega_p$ ,  $\omega_s = \omega_p - \omega_c$ ,  $\omega_b = -5\omega_c$ ,  $\omega_m = -0.5\omega_c$ , and  $\omega_e = 0.5\omega_c$ .

probability from the initial state  $|b, 0\rangle$  to the final state  $|b, 1\rangle$  as

$$P_1 = \frac{4\alpha^2 |\sin\theta_1|^2 |\cos\theta_1|^2}{(|\sin\theta_1|^2 + \alpha^2 |\cos\theta_1|^2)^2} \sin^4 \frac{\bar{\omega}t}{2} \quad (16)$$

where the effective frequency is defined as  $\bar{\omega} = (\Omega_p/2)\sqrt{|\sin\theta_1|^2 + \alpha^2 |\cos\theta_1|^2}$ . When the intensity ratio of the two driving fields reaches the optimal value

$$\alpha = \alpha_c = \frac{|\sin\theta_1|}{|\cos\theta_1|}, \quad (17)$$

the population of state  $|b, 1\rangle$  achieves unity ( $P_1 = 1$ ) at time  $t = \pi/\bar{\omega}$ .

For the closed system, we have derived the effective Hamiltonian under both resonant and large-detuned driving. The exact numerical dynamics show well agreement with the analytical results, which is shown in Appendix A. Moreover, we observed that the population can be fully transferred from the initial state  $|b, 0\rangle$  to the final state  $|b, 1\rangle$  in either resonant or large-detuned driving, confirming the feasibility of our physical mechanism for creating single photons.

### III. SINGLE PHOTONS VIA STRONG COUPLING

In the previous section, we have investigated the generation of single photons under non-dissipative conditions. In this section, we focus on how the cavity photons can be transmitted out the cavity as real photons for  $g/\omega_c < 0.1$ . The dynamics of the open system is governed by the master equation at zero temperature [36]

$$\frac{d\rho(t)}{dt} = i[\rho(t), H] + \mathcal{L}_1\rho + \mathcal{L}_2\rho + \mathcal{L}_3\rho, \quad (18)$$

where

$$\begin{aligned} \mathcal{L}_1\rho &= \kappa_1 (2|m\rangle\langle e|\rho|e\rangle\langle m| - |e\rangle\langle e|\rho - \rho|e\rangle\langle e|), \\ \mathcal{L}_2\rho &= \kappa_2 (2|b\rangle\langle m|\rho|m\rangle\langle b| - |m\rangle\langle m|\rho - \rho|m\rangle\langle m|), \\ \mathcal{L}_3\rho &= \kappa_3 (2a\rho a^\dagger - a^\dagger a\rho - \rho a^\dagger a), \end{aligned} \quad (19)$$

and  $\kappa_1$  and  $\kappa_2$  denote the damping rate associated with the decay from  $|e\rangle$  to  $|m\rangle$  and from  $|m\rangle$  to  $|b\rangle$  respectively, and  $\kappa_3$  is the cavity decay rate.

To investigate the quantum statistical behavior of the system, we calculate the time-delayed second-order correlation function [37]

$$g^{(2)}(\tau) = \frac{\langle a^\dagger(t)a^\dagger(t+\tau)a(t+\tau)a(t) \rangle}{\langle a^\dagger(t)a(t) \rangle \langle a^\dagger(t+\tau)a(t+\tau) \rangle}. \quad (20)$$

We first investigate continuous driving case. The dependence of the equal-time second-order correlation function  $g^{(2)}(0)$  on the driving amplitude  $\Omega_p$ , the coupling strength  $g$  and the damping rate is shown in Fig. 2. Here, we select the time  $t$  at the first peak of the photon number  $\bar{n}(t)$  [38, 39]. Fig.2(a) shows the dependence on  $\Omega_p$  with  $g/\omega_c = 0.05$  and  $\kappa_i/\omega_c = \kappa/\omega_c = 1 \times 10^{-3}$ ,  $8 \times 10^{-4}$  and  $5 \times 10^{-4}$ , respectively.  $g^{(2)}(0)$  increases with increasing  $\Omega_p$  for various damping rate. Based on this phenomenon, we further investigate the dependence of  $g^{(2)}(0)$  on  $g$  and  $\kappa$  in Fig.2(b) by setting  $\Omega_p = 0.001\omega_c$ . As shown in Fig. 2(b),  $g^{(2)}(0)$  decreases with the increase of  $g$ . Meanwhile, the dependence of  $g^{(2)}(0)$  on dissipation is not monotonic due to the competition with coupling strength  $g$ . As indicated by the black and white dashed curves in Fig. 2(b),  $g^{(2)}(0)$  remains on the order of  $10^{-3}$  when  $\kappa/\omega_c < 2 \times 10^{-3}$  and  $0.025 < g/\omega_c < 0.1$ , and even reaches the order of  $10^{-4}$  when  $\kappa/\omega_c < 6 \times 10^{-6}$  and  $0.07 < g/\omega_c < 0.10$ . For example, at  $\kappa/\omega_c = 10^{-6}$  and  $g/\omega_c = 0.08$ ,  $g^{(2)}(0) = 5.41 \times 10^{-4}$ . After normalizing the maximum value of  $g^{(2)}(\tau)$ , we obtain  $g^{(2)}(0) = 5.27 \times 10^{-6}$ , which is four orders of magnitude smaller than the result reported in Ref. [38, 40]. This demonstrates a significantly strong antibunching effect.

To see clearly the single-photon emission dynamics, we further plot the evolution of the mean photon number  $\bar{n}(t) = \langle a^\dagger(t)a(t) \rangle$  in Fig. 3(a). When  $\kappa/\omega_c = 10^{-6}$ , and  $g/\omega_c = 0.08$ , it is clearly observed that the photon number exhibits coherent oscillations between 0 and 1 accompanied by a slowly reducing of amplitude. Specifically, the amplitudes of the first three oscillation peaks were 0.993, 0.98, and 0.969 respectively, and eventually decayed to a stable value. This phenomenon reveals that single photons can be emitted at  $t = nT$  with periodicity  $T \approx 1.26 \times 10^{-2}/\kappa$ . When the system reaches a steady state, the system is in the coherent superposition of  $|b, 0\rangle$  and  $|b, 1\rangle$ . This indicates that, under weak continuous driving, the system evolves into a dynamically balanced steady state. This confirms that the two or more photons are completely suppressed. To further verify the analysis, we plot the normalized  $g^{(2)}(\tau)$  in Fig. 3(b) using the same parameters as in Fig. 3(a). Here we normalize  $g^{(2)}(\tau)$  by the maximum amplitude of its peak.

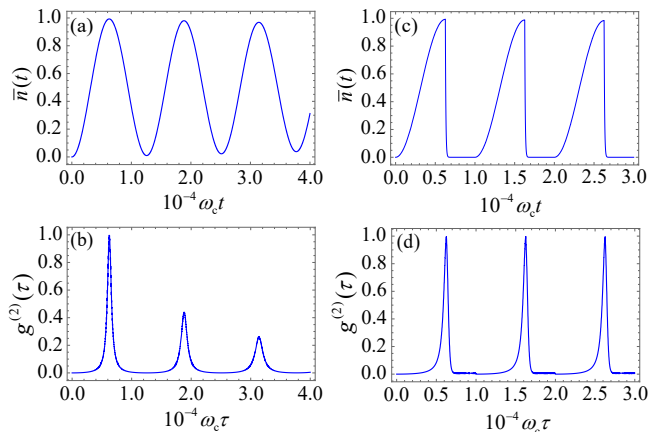


FIG. 3. (Color online) (a, c) Time evolution of the average photon number  $\bar{n}(t)$  under (a) continuous driving and (c) pulse driving, respectively. (b, d) Normalized second-order correlation function  $g^{(2)}(\tau)$  as a function of the delay time  $\tau$  under (b) continuous driving and (d) pulse driving, respectively. The parameters are set as: (a, b)  $\kappa_i = 10^{-6}\omega_c$  ( $i = 1, 2, 3$ ) and (c, d)  $T = 10^4/\omega_c$ ,  $\kappa_0 = 10^{-6}\omega_c$  and  $\kappa' = 8 \times 10^{-3}\omega_c$  with  $\delta = 0$ ,  $\Omega_p = 10^{-3}\omega_c$  and  $g = 0.08\omega_c$ . Other parameters are the same as in Fig. 2.

It is found that  $g^{(2)}(0) = 5.27 \times 10^{-6}$ , and  $g^{(2)}(\tau)$  exhibit multi peaks with the same periodicity with  $\bar{n}(t)$  and height reducing apparently. The locations of each peaks of  $g^{(2)}(\tau)$  matches well with that of  $\bar{n}(t)$ . These peaks denote individual single-photon emission events. We point out that, the probability on multi-photons are not strongly suppressed for the off-resonance driving in a long time due to two- or more-photon processes involved for  $g/\omega_c < 0.1$ .

Then, we explore the indistinguishability  $I$  of the single-photon source, which is a fundamental parameter characterizing whether quantum interference between photons can occur. To quantify indistinguishability, we analyze the delayed second-order correlation function  $g^{(2)}(\tau)$ . Specifically, we extract the area of the central peak around  $\tau = 0$ , divide it by the area of the unattenuated side peaks, and subtract this ratio from 1 [41]. A value closer to 1 indicates higher photon indistinguishability, reflecting better single-photon source quality. As shown in Fig. 3(b),  $I = 98.73\%$ , which approaches 100%. Another metric is the purity  $P$ , which is defined as [42]

$$P = 1 - g^{(2)}(0). \quad (21)$$

The corresponding purity  $P = 99.95\%$  in Fig. 3(b).

To better generate single photons, we apply pulse driving instead of continuous driving. Specifically, we turn on and off the driving fields and varying the cavity damping rate periodically, which follows the forms

$$\Omega_i(t) = \Omega_i \sum_{n=0}^{\infty} [\Theta(t - nT) - \Theta(t - nT - t_1)], (i = p, s), \quad (22)$$

$$\begin{aligned} \kappa_3(t) = & \sum_{n=0}^{\infty} \kappa_0 [\Theta(t - nT) - \Theta(t - nT - t_1)] + \\ & \sum_{n=0}^{\infty} \kappa' [\Theta(t - nT - t_1) - \Theta(t - nT - T)], \end{aligned} \quad (23)$$

where  $\Theta$  is the Heaviside step function.  $T$  is the periodicity of one emission cycle. To be different from continuous driving, we change the notations  $\Omega_i \rightarrow \Omega_i(t)$  and  $\kappa_3 \rightarrow \kappa_3(t)$ . For strong coupling,  $t_1 \approx \pi/(2g_{0,1})$  (detuned) and  $\pi/\bar{\omega}$  (resonant) is the moment of the first peak of  $\bar{n}(t)$ . At time  $t = t_1$ , the driving fields are first turned off and the cavity decay rate  $\kappa_3$  is simultaneously adjusted from  $\kappa_0$  to a higher value  $\kappa'$  to let single photons emit quickly [43]. After photons emitted, the system returns back to the ground state. Then the driving fields are turned on again at time  $t = T$ , beginning the second cycle with the above steps repeated. The above single-photon generation and emission processes are periodically repeated. We numerically simulate  $\bar{n}(t)$  and  $g^{(2)}(\tau)$  for this pulse driving scheme in Fig. 3(c) and 3(d), respectively. It is observed that  $\bar{n}(t)$  oscillates periodically between 0 and 1, with  $T = 10^4/\omega_c$ . Meanwhile,  $g^{(2)}(\tau)$  shows coherent oscillations with the same period as  $\bar{n}(t)$ , which is a clear signature of single-photon source. Importantly, the height of all the peaks becomes the same. The corresponding single-photon efficiency [39]

$$\varepsilon = \kappa_3 \int \langle a^\dagger(t)a(t) \rangle dt, \quad (24)$$

is 50%, the indistinguishability  $I$  is 98.47%, and the purity  $P$  remains consistent with that under continuous driving, i.e.,  $P = 99.95\%$ .

#### IV. SINGLE PHOTONS VIA ULTRA STRONG COUPLING

In this section, we further explore the ultrastrong coupling regime where  $g/\omega_c > 0.1$ . Under the conditions of weak system–bath coupling, short bath correlation time and the conventional Born–Markov approximation [36], the dynamics of the open quantum system in the ultrastrong coupling regime is governed by the following master equation [44, 45]:

$$\begin{aligned} \frac{d\rho(t)}{dt} = & i[\rho(t), H] \\ & + \sum_{i=1}^3 \sum_{n, m > n} \Gamma_{mn}^{(i)} \{ \mathcal{D}[|E_n\rangle\langle E_m|] \rho(t) \} \end{aligned} \quad (25)$$

The dissipative superoperator is defined as  $\mathcal{D}[O]\rho = O\rho O^\dagger - \frac{1}{2}O^\dagger O\rho - \frac{1}{2}\rho O^\dagger O$ . Here,  $\{E_n\} = \{|b, 0\rangle, |b, 1\rangle, \dots, |\varepsilon_0\rangle, |\varepsilon_1\rangle, \dots\}$  are the eigenstates of  $H_0$ , satisfying  $H_0|E_n\rangle = E_n|E_n\rangle$ . The index

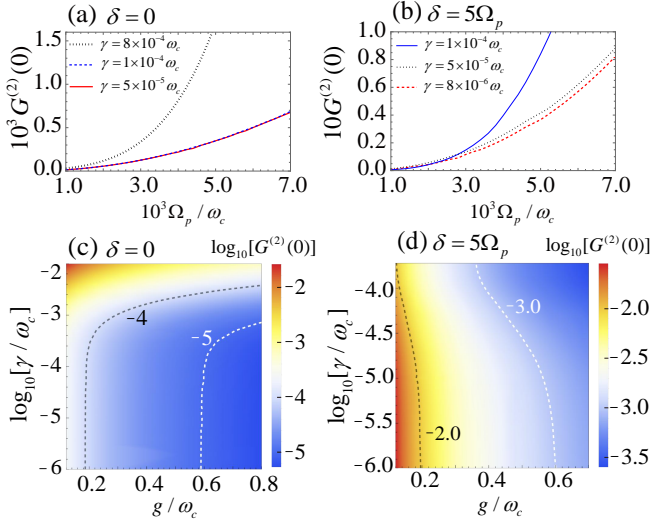


FIG. 4. (Color online) (a, b) Equal-time second-order correlation function  $G^{(2)}(0)$  as a function of the driving amplitude  $\Omega_p$  with  $g = 0.5\omega_c$  for (a) resonant case ( $\delta = 0$ ) at  $\gamma_i = \gamma = 8 \times 10^{-4}\omega_c$  ( $i = 1, 2, 3$ ) (black dotted curve),  $1 \times 10^{-4}\omega_c$  (blue dashed curve) and  $5 \times 10^{-5}\omega_c$  (red solid curve), and (b) detuned case ( $\delta = 5\Omega_p$ ) at  $\gamma = 1 \times 10^{-4}\omega_c$  (blue solid curve),  $5 \times 10^{-5}\omega_c$  (red dashed curve), and  $8 \times 10^{-6}\omega_c$  (black dotted curve). (c, d)  $G^{(2)}(0)$  vs the coupling strength  $g$  and the decay rate  $\gamma$  for  $\Omega_p = 1 \times 10^{-3}\omega_c$  at (c) resonant case ( $\delta = 0$ ) and (d) detuned case ( $\delta = 5\Omega_p$ ). The white and black dashed curves in (c) correspond to  $G^{(2)}(0) = 10^{-5}$  and  $G^{(2)}(0) = 10^{-4}$ , and those in (d) correspond to  $G^{(2)}(0) = 10^{-2}$  and  $G^{(2)}(0) = 10^{-3}$ . Other common parameters are:  $\Omega_s = \alpha\Omega_p$ ,  $\omega_s = \omega_p - \omega_c$ ,  $\omega_b = -5\omega_c$ ,  $\omega_m = -0.5\omega_c$  and  $\omega_e = 0.5\omega_c$ .

$i = 1, 2, 3$  labels three independent dissipation channels:  $i = 1$  represents atomic decay from the excited state  $|e\rangle$  to the intermediate state  $|m\rangle$ ,  $i = 2$  describes the decay from  $|m\rangle$  to the ground state  $|b\rangle$ , and  $i = 3$  accounts for cavity photon damping induced by transmission losses. The relaxation rate  $\Gamma_{mn}^{(i)}$  takes the form

$$\Gamma_{mn}^{(i)} = 2\pi\varrho^{(i)}(\omega_{nm})\lambda_j^{(i)2}(\omega_{nm})|C_{nm}^{(i)}|^2. \quad (26)$$

In the above expression,  $\omega_{nm} = E_n - E_m$  is the transition frequency between eigenstates  $|E_n\rangle$  and  $|E_m\rangle$ ,  $\varrho^{(i)}(\omega_{nm})$  is the spectral density of the  $i$ -th reservoir at frequency  $\omega_{nm}$ ,  $\lambda^{(i)}(\omega_{nm})$  characterizes the system–bath coupling strength, and  $C_{n,m}^{(i)}$  denotes the corresponding transition matrix element. The explicit forms of  $C_{n,m}^{(i)}$  are presented below:

$$C_{nm}^{(1)} = \langle E_n | (|e\rangle\langle m| + |m\rangle\langle e|) | E_m \rangle, \quad (27)$$

$$C_{nm}^{(2)} = \langle E_n | (|m\rangle\langle b| + |b\rangle\langle m|) | E_m \rangle, \quad (28)$$

$$C_{nm}^{(3)} = \langle E_n | (a + a^\dagger) | E_m \rangle. \quad (29)$$

In the derivation of Eq. (25), we neglect the Lamb-shift induced corrections to the system energy levels. To simplify the analysis, we assume that the coupling strength

$\lambda^{(i)}(\omega_{nm})$  and the spectral density of the environment  $\varrho^{(i)}(\omega_{nm})$  are constants within the relevant frequency range. Under this assumption, the relaxation coefficient can be simplified as  $\Gamma_{mn}^{(i)} = \gamma_i |C_{nm}^{(i)}|^2$ .

To study the statistical properties of the emitted photons, we need to employ the input-output theory in the ultrastrong coupling regime[45, 46]. Then, we numerically examine the second-order correlation function defined by

$$G^{(2)}(\tau) = \frac{\langle X^+(t)X^+(t+\tau)X^-(t+\tau)X^-(t) \rangle}{\langle X^+(t)X^-(t) \rangle \langle X^+(t+\tau)X^-(t+\tau) \rangle}. \quad (30)$$

The cavity mode operator  $a(a^\dagger)$  has been replaced by the operator  $X^-(X^+)$  defined as

$$X^- = \sum_{m,n < m} C_{n,m}^{(3)} |E_n\rangle\langle E_m|, \quad (31)$$

$$X^+ = (X^-)^\dagger, \quad (32)$$

which describes the transition between the eigenstates of the ultrastrongly coupled system. To be practical, we select time  $t$  in  $G^{(2)}(\tau)$  the moment when the photon number  $\langle X^+X^- \rangle$  reaches its first maximum, namely when the first photon is emitted.

We first study the continuous driving scheme. We investigated the dependence of  $G^{(2)}(0)$  on the driving amplitude  $\Omega_p$  in both resonant and detuned cases at  $g/\omega_c = 0.5$ , and show the results in Figs. 4(a) and 4(b). It can be observed that, whether in the resonant case ( $\delta = 0$ ) or the detuned case ( $\delta = 5\Omega_p$ ),  $G^{(2)}(0)$  monotonically increases with the increase of  $\Omega_p$  under various decay rates. With the guidance of the above result, we further explore the dependence of  $G^{(2)}(0)$  on the coupling strength  $g$  and the decay rate  $\gamma_i = \gamma$  ( $i = 1, 2, 3$ ) at  $\Omega_p = 1 \times 10^{-3}\omega_c$  and show the results in Figs. 4(c) and 4(d) for resonant and detuned cases, respectively. Observation reveals that in both resonant and detuned cases,  $G^{(2)}(0)$  decreases as the coupling strength  $g$  increases, but it has a non-monotonic dependence on the decay rate  $\gamma$ . This non-monotonicity stems from the competition between  $g$  and  $\gamma$ . In both the resonant and detuned cases, as the dissipation  $\gamma$  increases, the coupling between the cavity mode and the external thermal reservoir is strengthened, leading to a shortened cavity photon lifetime and a reduced average photon number. Consequently, the average photon number in the cavity decreases correspondingly with increasing dissipation. When the system is dissipationless, multiphoton processes gradually emerge over time under detuned conditions; however, the introduction of dissipation causes the system to decay downward before upward transitions can occur, thereby effectively suppressing the accumulation of multiphotons. Based on the above analysis, we need to choose an appropriate decay rate to balance this effect. In the resonant case with  $\delta = 0$  corresponding to Fig. 4(c), the black dashed curve shows that  $G^{(2)}(0) = 10^{-4}$  for ( $g/\omega_c \sim 0.18, \gamma/\omega_c \sim 10^{-6}$ ) or ( $g/\omega_c \sim 0.8, \gamma/\omega_c \sim$

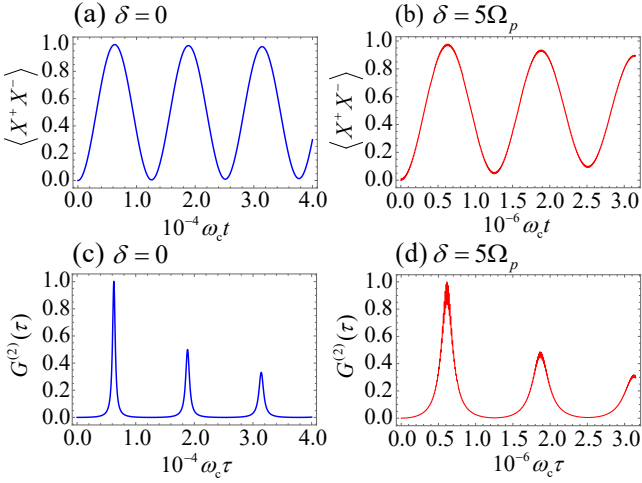


FIG. 5. (a, b) Time evolution of the average photon number  $\langle X^+ X^- \rangle$  for (a) resonant case ( $\delta = 0$ ) and (b) detuned case ( $\delta = 5\Omega_p$ ). (c, d) Normalized second-order correlation function  $G^{(2)}(\tau)$  vs  $\tau$  for (c) resonant case ( $\delta = 0$ ) and (d) detuned case ( $\delta = 5\Omega_p$ ). The common parameters are  $\gamma = 10^{-6}\omega_c$  and  $g = 0.7\omega_c$ . Other parameters are the same as in Fig. 4.

$4 \times 10^{-3}$ ), while the white dashed curve indicates that  $G^{(2)}(0) = 10^{-5}$  for ( $g/\omega_c \sim 0.58, \gamma/\omega_c \sim 10^{-6}$ ) or ( $g/\omega_c \sim 0.8, \gamma/\omega_c \sim 7 \times 10^{-4}$ ). For the detuned case of  $\delta = 5\Omega_p$  in Fig. 4(d), the white dashed curve presents  $G^{(2)}(0) = 10^{-3}$  for ( $g/\omega_c \sim 0.36, \gamma/\omega_c \sim 1.9 \times 10^{-4}$ ) or ( $g/\omega_c \sim 0.6, \gamma/\omega_c \sim 10^{-6}$ ). These results strongly demonstrate the realization of a single-photon source operating in the ultrastrong coupling regime. Specifically, for the parameter set ( $g/\omega_c, \gamma/\omega_c$ ) = (0.7,  $10^{-6}$ ) in Fig. 4(c), the calculated  $G^{(2)}(0)$  is  $7.09 \times 10^{-6}$ , which is further reduced to  $3.32 \times 10^{-8}$  after normalization. For detuned driving with  $\delta = 5\Omega_p$ , the same parameter point delivers a  $G^{(2)}(0)$  of  $7.31 \times 10^{-4}$ , and the normalized result is  $3.41 \times 10^{-5}$ . To the best of our knowledge, previous investigations on cavity QED systems have only achieved a minimum  $G^{(2)}(0)$  of  $10^{-2}$ . Notably, our optimized results are six orders of magnitude lower than those reported in prior studies [39, 42, 47].

To be more clear, we further plot the time evolution of the average photon number  $\langle X^+ X^- \rangle$  and normalized  $G^{(2)}(\tau)$  in Fig. 5 by the same parameters  $g/\omega_c$  and  $\gamma/\omega_c$  discussed above, namely, ( $g/\omega_c, \gamma/\omega_c$ ) = (0.7,  $10^{-6}$ ). As shown in Figs. 5(a) and 5(b), the average cavity photon number  $\langle X^+ X^- \rangle$  oscillates periodically between 0 and 1 with a very slowly reducing amplitude. The oscillation period  $T \approx 1.26 \times 10^{-2}/\gamma$  in Fig. 5(a) and  $T \approx 0.13/\gamma$  in Fig. 5(b) respectively. The values of first and third peaks are 0.996 and 0.98 in Fig. 5(a), and 0.976 and 0.897 in Fig. 5(b). The amplitudes of  $\langle X^+ X^- \rangle$  eventually reaches a steady value in a long enough time with a steady state of a superposition  $|b, 0\rangle$  and  $|b, 1\rangle$ . This indicates that the system can continuously generate single photons under continuous-wave driving. However, in the time we concern, there are al-

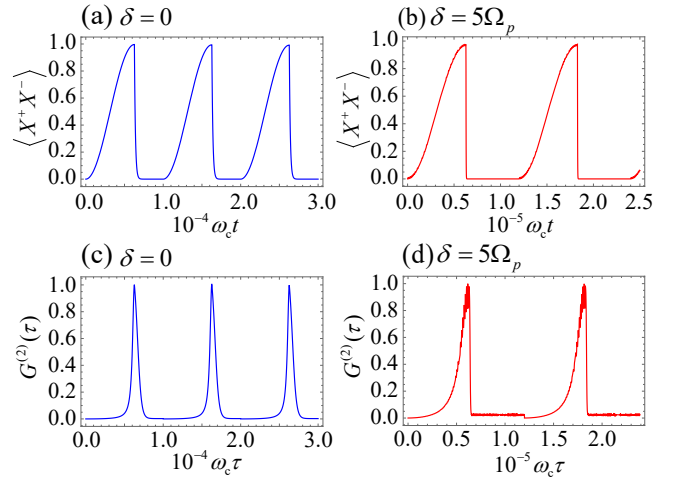


FIG. 6. Evolution of  $\langle X^+ X^- \rangle$  and  $G^{(2)}(\tau)$  with the driving fields  $\Omega_{p,s}$  periodically turned on at  $t = nT/\omega_c$  ( $n = 0, 1, 2, 3, \dots$ ) and off at the peaks of  $\langle X^+ X^- \rangle$ , accompanied by switching the cavity decay rate  $\gamma_3$  from  $\gamma_0 = 10^{-6}\omega_c$  to  $\gamma' = 8 \times 10^{-3}\omega_c$  simultaneously. (a, c) Resonance case ( $\delta = 0$ ) with periodicity  $T = 10^4/\omega_c$ ; (b, d) Detuned case ( $\delta = 5\Omega_p$ ) with periodicity  $T = 1.2 \times 10^5/\omega_c$ . Other parameters are the same as in Fig. 5.

ready enough peaks occur that indicate the generation of single-photons. This observation can be further verified in Figs. 5(c) and 5(d), where  $G^{(2)}(\tau)$  is normalized. As shown in Figs. 5(c) and 5(d),  $G^{(2)}(0) = 3.32 \times 10^{-8}$  (Fig. 5(c)) and  $3.41 \times 10^{-5}$  (Fig. 5(d)) respectively, which are much less than 0.1, indicating a significant photon anti-bunching phenomenon. This is a clear characteristic of single photon emission. Moreover,  $G^{(2)}(\tau)$  periodically oscillates and exhibits much peaks with height reducing apparently. The locations of the peaks just match well with the peaks of  $\langle X^+ X^- \rangle$  in Figs. 5(a) and 5(b) respectively. Every time the photon number approaches its maximum, a single-photon emission occurs and  $G^{(2)}(\tau)$  reaches maximum. Then, the system returns to the initial state  $|b, 0\rangle$ . Under continuous driving the system transfers to  $|b, 1\rangle$  from  $|b, 0\rangle$  again and begins another photon emission cycle. The above processes repeats periodically, demonstrating periodic single-photon release. We also note that the summation of the probabilities on  $|b, 0\rangle$  and  $|b, 1\rangle$  is almost 1 during the above process. To evaluate the performance of the single photon source, we further analyze the indistinguishability  $I$  of the emitted photons. Here  $I$  is obtained by the similar formula in the strong coupling regime but replacing  $g^{(2)}(\tau)$  by  $G^{(2)}(\tau)$ . As shown in Figs. 5(c) and 5(d), the indistinguishability of the emitted photons is 99.10% and 96.10% respectively, which is close to 100%. Our scheme works well for both resonant and detuned case in the ultrastrong coupling regime.

To collect single photons, we apply the same pulse driving as in Eq. (23), but replace the cavity decay rate  $\kappa_3(t), \kappa_0, \kappa'$  by  $\gamma_3(t), \gamma_0$  and  $\gamma'$ .  $t_1$  is the moment

of the first peak of  $\langle X^+ X^- \rangle$ . Using the same parameters as in Fig. 5, we numerically simulate  $\langle X^+ X^- \rangle$  and  $G^{(2)}(\tau)$  for  $T = 10^4/\omega_c$  (resonant) and  $T = 1.2 \times 10^5/\omega_c$  (detuned) and show the results in Fig. 6. As shown in Figs. 6(a) and 6(b),  $\langle X^+ X^- \rangle$  periodically oscillates between 0 and 1 for both resonant and detuned cases. The normalized  $G^{(2)}(\tau)$  [Figs. 6(c) and 6(d)] shares the same period as  $\langle X^+ X^- \rangle$ , featuring peaks with the identical height.  $G^{(2)}(0) = 3.32 \times 10^{-8}$  and  $G^{(2)}(0) = 3.41 \times 10^{-5}$ , which is approaching zero. This is clear evidence of single photon source. To evaluate the performance of the single photon source, we explore the single-photon efficiency, defined as

$$\epsilon = \gamma_3 \int \langle X^+(t) X^-(t) \rangle dt. \quad (33)$$

$\epsilon$  reaches 99.96% and 100% for the resonant and detuned cases, respectively. The corresponding indistinguishability  $I$  are 98.98% (resonant) and 95.91% (detuned), respectively. The purity  $P$  remains the same as the continuous-wave driving case, namely  $P = 99.99\%$  (resonant) and  $P = 99.93\%$  (detuned). Therefore, the system exhibits excellent performance for single-photon source in the ultrastrong coupling regime.

## V. DISCUSSION AND CONCLUSION

We discuss the experimental feasibility of the proposed scheme, whose key experimental prerequisites are the realization of the ultrastrong Jaynes–Cummings (JC) model and the implementation of a  $\Delta$ -type atomic configuration. Notably, our scheme is applicable to both strong and ultrastrong coupling regimes, which significantly enhances its experimental flexibility. The ultrastrong coupling regime has been experimentally realized on multiple state-of-the-art platforms, including superconducting circuits [48–51], Landau polaritons [52–55], organic molecules [56–58], optomechanical systems [59], and intersubband polaritons [60–62]. Impressively, deep-strong coupling with  $g/\omega_c = 1.34$  and  $g/\omega_c = 1.43$  has been reported in circuit QED systems and semiconductor quantum wells, respectively [51, 52]. The effective ultrastrong JC model can be derived from the full quantum Rabi model by dynamically suppressing counter-rotating terms via external field modulation [32, 33, 63]. In addition, exact JC-type coupling can be naturally established when the two upper atomic levels feature an angular momentum difference of  $\Delta m = \pm 1$  and interact with circularly polarized optical fields [31]. Regarding the  $\Delta$ -type cyclic atomic configuration, such closed-transition structures are absent in natural atoms due to inherent selection rules. Nevertheless, they can be faithfully implemented in symmetry-broken quantum systems, such as chiral molecules [25–27] and artificially engineered quantum atoms with broken symmetry [28]. In particular, the  $\Delta$ -type artificial atom has been experimentally demonstrated in superconducting quantum circuits [29].

Furthermore, the dissipative parameters adopted in our model are also experimentally accessible. The cavity decay rate  $\kappa/\omega_c$  and atomic decay rate  $\gamma/\omega_c$  ranging from  $10^{-6}$  to  $10^{-3}$  have been achieved in various cavity QED [65?] and circuit QED platforms [66, 67]. Moreover, dynamical tuning of the cavity decay rate has been experimentally validated in previous works [43]. Collectively, all the required physical conditions and key parameters of our scheme are achievable with current experimental technologies, confirming the practical experimental accessibility of the proposed deterministic single-photon source.

We propose a practical scheme for a deterministic single-photon source based on a  $\Delta$ -type three-level atom coupled to a single-mode cavity field. By applying two classical driving fields, deterministic single-photon emission can be generated in both strong and ultrastrong coupling regimes. For continuous-wave driving, the system exhibits excellent single-photon performance. In the strong coupling regime, the normalized equal-time second-order correlation function is  $g^{(2)}(0) \sim 10^{-6}$ , with a photon indistinguishability of 98.73% and a state purity of 99.95%. In the ultrastrong coupling regime, the corresponding normalized equal-time second-order correlation function is  $G^{(2)}(0) \sim 10^{-8}$ , achieving an indistinguishability of 99.10% and a purity of 99.99%. For pulsed driving within the ultrastrong coupling regime, the emission efficiency, indistinguishability, and purity reach 99.96%, 98.98%, and 99.99% under resonant conditions, and 100%, 95.91%, and 99.93% under detuned conditions, respectively. The near-perfect performance of the proposed single-photon source addresses the long-standing challenge in linear optical quantum computing. This work provides a feasible route for the implementation of deterministic single-photon sources, promotes the advancement of quantum information science, and deepens the physical understanding of fundamental quantum mechanisms.

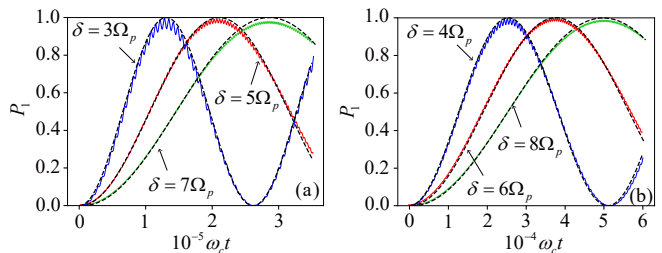


FIG. 7. (Color online) Population  $P_1$  of state  $|b, 1\rangle$  versus time, obtained from the effective Hamiltonian (12) (black dashed lines) and the exact Hamiltonian (7) (solid lines) for multiple detunings in the (a) strong-coupling and (b) ultrastrong-coupling regimes. Parameters: (a)  $g = 0.06\omega_c$ ,  $\Omega_p = 3 \times 10^{-4}\omega_c$ ,  $\delta = 3\Omega_p$  (blue),  $5\Omega_p$  (red), and  $7\Omega_p$  (green); (b)  $g = 0.5\omega_c$ ,  $\Omega_p = 2 \times 10^{-3}\omega_c$ ,  $\delta = 4\Omega_p$  (blue),  $6\Omega_p$  (red), and  $8\Omega_p$  (green). Common parameters:  $\Omega_s = \alpha\Omega_p$ ,  $\omega_s = \omega_p - \omega_c$ ,  $\omega_b = -5\omega_c$ ,  $\omega_m = -0.5\omega_c$ , and  $\omega_e = 0.5\omega_c$ . All parameters are given in units of  $\omega_c$ .

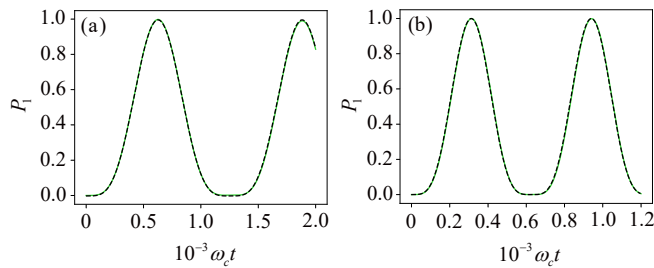


FIG. 8. (Color online) Time evolution of the single-photon occupation probability  $P_1$  of state  $|b, 1\rangle$  at resonance ( $\delta = 0$ ). Black dashed curves: effective Hamiltonian Eq. (15); green solid curves: full numerical simulations of the exact Hamiltonian Eq. (7). Results are shown for (a) strong-coupling and (b) ultrastrong-coupling regimes. (a)  $g = 0.05\omega_c$ ,  $\Omega_p = 10^{-3}\omega_c$  and  $\alpha = \alpha_c$ . (b)  $g = 0.5\omega_c$ ,  $\Omega_p = 2 \times 10^{-3}\omega_c$  and  $\alpha = \alpha_c$ . The rest of the parameters are the same as Fig. 7.

## ACKNOWLEDGMENTS

We gratefully acknowledge Jie Peng for technical support. J.-F. H. is partially supported by the National Natural Science Foundation of China (Grant No. 12475016) and the Science and Technology Innovation Program of Hunan Province (Grant No. 2025RC3141).

### Appendix A: Validity of the effective Hamiltonian (12) and (15)

To show the validity of the effective Hamiltonian (12) and (15), we calculate the probability  $P_1$  in state  $|b, 1\rangle$  from initial state  $|b, 0\rangle$  for strong and ultrastrong coupling regimes, respectively. Then we compare the results with that numerically obtained from the exact Hamiltonian (7) for large detuning and resonant cases respectively.

#### 1. Large detuning case

To verify the validity of the effective Hamiltonian (12), we calculate the probability  $P_1$  from both effective Hamiltonian (12) and exact Hamiltonian (7) with the large detuning condition  $\varepsilon_1 - \omega_b - \omega_p \gg \chi_p$  and  $\varepsilon_1 - \omega_b - \omega_c - \omega_s \gg \chi_s$ .

Fig. 7 presents the analytical and numerical results in both strong ( $g/\omega_c = 0.06$ ) and ultrastrong ( $g/\omega_c = 0.5$ ) coupling regimes. By varying the detuning  $\delta$ , the numerical results were compared with the predictions of the effective Hamiltonian (12), as depicted in Fig. 7. Figure 7(a) shows that a complete Rabi oscillations predicted by the effective Hamiltonian (12) are in good agreement with the numerical results in strong coupling regime. As the detuning increases, a 4% deviation is observed at  $\delta = 7\Omega_p$ . This deviation arises because an increase in detuning reduces the difference between the effective coupling strengths  $g_{0,1}$  and  $g_{1,2}$ , which in turn weakens the system's ability to suppress multiphoton transitions. When the coupling strength enters the ultrastrong coupling region, as shown in Fig. 7(b), the analytical and numerical solutions are highly consistent, achieving perfect state transfer between the states  $|b, 0\rangle$  and  $|b, 1\rangle$ . This phenomenon verify the physical mechanism to generate single photons since the atom state  $|b\rangle$  is decoupled from the cavity field. The results demonstrates that the exact Hamiltonian (7) can be well approximated by the effective Hamiltonian (12), which capture the main mechanism to generate single photons.

#### 2. Resonance case

We consider the resonant case:  $\varepsilon_1 - \omega_b - \omega_p = 0$  and  $\varepsilon_1 - \omega_b - \omega_c - \omega_s = 0$ . In order to verify the validity of the effective three-level Hamiltonian (15), we numerically calculate the evolution of  $P_1$  governed by Hamiltonian (7) from  $|b, 0\rangle$  for  $g = 0.05\omega_c$  and  $g = 0.5\omega_c$  respectively. Then we compared the exact results with analytical result Eq. (16) obtained from the effective Hamiltonian (15) in Fig. 8. Our results indicate that, the Rabi oscillation predicted by the effective Hamiltonian Eq. (15) is in well agreement with that predicted by the exact Hamiltonian (7) both in strong and ultrastrong coupling regimes. Moreover, when the ratio  $\alpha$  between the amplitudes of the driving fields reaches the optimal value  $\alpha = \alpha_c$ , the peak value of the probability  $P_1$  can reach 1, which confirms the perfect single-photon generation.

[1] M. A. Nielsen and I. L. Chuang, *Quantum Computation and Quantum Information* (Cambridge University Press, Cambridge, England, 2000).  
 [2] C. L. Degen, F. Reinhard, and P. Cappellaro, Quantum sensing, *Rev. Mod. Phys.* **89**, 035002 (2017).  
 [3] V. Giovannetti, S. Lloyd, and L. Maccone, Advances in quantum metrology, *Nat. Photonics* **5**, 222 (2011).  
 [4] J. L. O'Brien, A. Furusawa, and J. Vučković, Photonic quantum technologies, *Nature Photon* **3**, 687–695 (2009).

[5] X.-H. Zhan, Z.-Q. Zhong, J.-Y. Ma, S. Wang, Z.-Q. Yin, W. Chen, D.-Y. He, G.-C. Guo, Z.-F. Han, Experimental demonstration of long distance quantum communication with independent heralded single photon sources, *npj Quantum Inf.* **11**, 73 (2025).  
 [6] J. I. Cirac, P. Zoller, H. J. Kimble, and H. Mabuchi, Quantum State Transfer and Entanglement Distribution among Distant Nodes in a Quantum Network, *Phys. Rev. Lett.* **78**, 3221 (1997).

- [7] J. W. Pan, Z. B. Chen, C. Y. Lu, H. Weinfurter, A. Zeilinger, and M. Zukowski, Multiphoton entanglement and interferometry, *Rev. Mod. Phys.* **84**, 777 (2012).
- [8] J. Yin, Y. Cao, Y.-H. Li, S.-K. Liao, L. Zhang, J.-G. Ren, W.-Q. Cai, W.-Y. Liu, B. Li, H. Dai, G.-B. Li, Q.-M. Lu, Y.-H. Gong, Y. Xu, S.-L. Li, F.-Z. Li, Y.-Y. Yin, Z.-Q. Jiang, M. Li, J.-J. Jia, G. Ren, D. He, Y.-L. Zhou, X.-X. Zhang, N. Wang, X. Chang, Z.-C. Zhu, N.-L. Liu, Y.-A. Chen, C.-Y. Lu, R. Shu, C.-Z. Peng, J.-Y. Wang, and J.-W. Pan, Satellite-based entanglement distribution over 1,200 kilometers, *Science* **356**, 1140 (2017).
- [9] X. R. Mao, W.-J. Ji, S.-L. Wang, H.-Q. Liu, B. Wu, X.-J. Wang, L. Liu, L. Zhou, H.-Q. Ni, Z.-C. Niu, Z.-L. Yuan, A single-photon source based on topological bulk cavity, *Light Sci. Appl.* **14**, 295 (2025).
- [10] X. Ding, Y.-P. Guo, M.-C. Xu, R.-Z. Liu, G.-Y. Zou, J.-Y. Zhao, Z.-X. Ge, Q.-H. Zhang, H.-L. Liu, L.-J. Wang, M.-C. Chen, H. Wang, Y.-M. He, Y.-H. Huo, C.-Y. Lu and J.-W. Pan, High-efficiency single-photon source above the loss-tolerant threshold for efficient linear optical quantum computing, *Nat. Photonics* **19**, 387 (2025).
- [11] E. Knill, R. Laflamme, and G. J. Milburn, A scheme for efficient quantum computation with linear optics, *Nature (London)* **409**, 46 (2001).
- [12] P. Kok, W. J. Munro, K. Nemoto, T. C. Ralph, J. P. Dowling, and G. J. Milburn, Linear optical quantum computing with photonic qubits, *Rev. Mod. Phys.* **79**, 135 (2007).
- [13] P. Lodahl, Quantum-dot based photonic quantum networks, *Quantum Sci. Technol.* **3**, 013001 (2018).
- [14] C.-Y. Lu and J.-W. Pan, Quantum-dot single-photon sources for the quantum internet, *Nat. Nanotechnol.* **16**, 1294 (2021).
- [15] B. Darquie, M. P. A. Jones, J. Dingjan, J. Beugnon, S. Bergamini, Y. Sortais, G. Messin, A. Browaeys, and P. Grangier, Controlled single-photon emission from a single trapped two-level atom, *Science* **309**, 454 (2005).
- [16] S. Shi, B. Xu, K. Zhang, G.-S. Ye, D.-S. Xiang, Y. B. Liu, J. Z. Wang, D. Q. Su, and L. Li, High-fidelity photonic quantum logic gate based on near-optimal Rydberg single-photon source, *Nat. Commun.* **13**, 4454 (2022).
- [17] C. Brunel, B. Lounis, P. Tamarat, and M. Orrit, Triggered Source of Single Photons based on Controlled Single Molecule Fluorescence, *Phys. Rev. Lett.* **83**, 2722 (1999)
- [18] P. Maunz, D. L. Moehring, S. Olmschenk, K. C. Younge, D. N. Matsukevich, and C. Monroe, Quantum interference of photon pairs from two remote trapped atomic ions, *Nat. Phys.* **3**, 538 (2007).
- [19] C. Kurtsiefer, S. Mayer, P. Zarda, and H. Weinfurter, Stable Solid-State Source of Single Photons, *Phys. Rev. Lett.* **85**, 290 (2000).
- [20] K. Parto, S. I. Azzam, K. Banerjee, and G. Moody, Defect and strain engineering of monolayer WSe<sub>2</sub> enables site-controlled single-photon emission up to 150 K. *Nat. Commun.* **12**, 3585 (2021).
- [21] C. Santori, M. Pelton, G. Solomon, Y. Dale, and Y. Yamamoto, Triggered Single Photons from a Quantum Dot, *Phys. Rev. Lett.* **86**, 1502 (2001).
- [22] T. Aichele, M. Scholz, and O. Benson, InP/GaInP quantum dots as single-photon sources for quantum information processing, *Proc. IEEE* **95**, 1791 (2007).
- [23] A. Gogyan, S. Guérin, H.-R. Jauslin, and Y. Malakyan, Deterministic source of a train of indistinguishable single-photon pulses with a single-atom-cavity system, *Phys. Rev. A* **82**, 023821 (2010).
- [24] M. E. Reimer and C. Cher, The quest for a perfect single-photon source, *Nat. Photon.* **13**, 734 (2019).
- [25] P. Král and M. Shapiro, Cyclic Population Transfer in Quantum Systems with Broken Symmetry, *Phys. Rev. Lett.* **87**, 183002 (2001).
- [26] P. Král, I. Thanopoulos, M. Shapiro, and D. Cohen, Two-Step Enantio-Selective Optical Switch, *Phys. Rev. Lett.* **90**, 033001 (2003).
- [27] Y. Li, C. Bruder, and C. P. Sun, Generalized Stern-Gerlach Effect for Chiral Molecules, *Phys. Rev. Lett.* **99**, 130403 (2007).
- [28] Y.-X. Liu, J. Q. You, L. F. Wei, C. P. Sun, and F. Nori, Optical Selection Rules and Phase-Dependent Adiabatic State Control in a Superconducting Quantum Circuit, *Phys. Rev. Lett.* **95**, 087001 (2005).
- [29] Z. H. Peng, Y.-X. Liu, J. T. Peltonen, T. Yamamoto, J. S. Tsai, and O. Astafiev, Correlated emission lasing in harmonic oscillators coupled via a single three-level artificial Atom, *Phys. Rev. Lett.* **115**, 223603 (2015).
- [30] E. T. Jaynes, and F. W. Cummings, Comparison of quantum and semiclassical radiation theories with application to the beam maser, *Proc. IEEE* **51**, 89 (1963).
- [31] M. D. Crisp, Jaynes-Cummings model without the rotating-wave approximation, *Phys. Rev. A* **43**, 2430 (1991).
- [32] J.-F. Huang, J.-Q. Liao, and L.-M. Kuang, Ultrastrong Jaynes-Cummings model, *Phys. Rev. A* **101**, 043835 (2020).
- [33] C. Liu and J.-F. Huang, Quantum phase transition of the Jaynes-Cummings model, *Sci. China Phys. Mech. Astron.* **67**, 210311 (2024).
- [34] D. F. James and J. Jerke, Effective Hamiltonian theory and its applications in quantum information, *Can. J. Phys.* **85**, 625 (2007).
- [35] W. J. Shao, C. F. Wu, and X.-L. Feng, Generalized James' effective Hamiltonian method, *Phys. Rev. A* **95**, 032124 (2017).
- [36] H. P. Breuer and F. Petruccione, *The Theory of Open Quantum Systems* (Oxford University Press, Oxford, 2002).
- [37] M. O. Scully and M. S. Zubairy, *Quantum Optics* (Cambridge University Press, Cambridge, 1997).
- [38] Y. Y. Yan, Y. B. Cheng, S. G. Guan, D. Y. Yu, and Z. L. Duan, Pulse-regulated single-photon generation via quantum interference in a  $\chi^{(2)}$  nonlinear nanocavity, *Opt. Lett.* **43**, 5086 (2018).
- [39] J. Peng, J. N. Tang, P. H. Tang, Z. Z. Ren, J. L. Tian, and N. Barraza, Deterministic single-photon source in the ultrastrong-coupling regime, *Phys. Rev. A* **108**, L031701 (2023).
- [40] X.-R. Mao, B. Wu, W.-J. Ji, S.-L. Wang, W.-Z. Li, H.-Q. Liu, H.-Q. Ni, Z.-C. Niu, and Z.-L. Yuan, Polarized Single-Photon Emission from an Anisotropic Dirac Cavity, *Phys. Rev. Lett.* **136**, 073603 (2026).
- [41] C. K. Hong, Z. Y. Ou, and L. Mandel, Measurement of Subpicosecond Time Intervals between Two Photons by Interference, *Phys. Rev. Lett.* **59**, 2044 (1987).
- [42] L. O. R. Solak, B. L. Vermes, A. S. M. de Castro, D. Z. Rossatto, and C. J. Villas-Boas, Quantum Resonator as a Directional Quantum Emitter, *Adv. Quantum Technol.* **8**, e2500710 (2025).

- [43] Y.-Z. Xiong, Z.-L. Wang, J.-W. Zhang, X.-D. Sun, Z.-H. Zhang, P.-S. Huang, Y.-Q. Liang, J. Jiang, J.-W. Qiu, Y.-X. Zhou, X.-Y. Linpeng, W.-H. Huang, J.-J. Niu, Y.-P. Zhong, J. Chu, S. Liu, and D.-P. Yu, High-performance multiplexed readout of superconducting qubits with a tunable broadband Purcell filter, *Phys. Rev. Appl.* **25**, 054010 (2026).
- [44] F. Beaudoin, J. M. Gambetta, and A. Blais, Dissipation and ultrastrong coupling in circuit QED, *Phys. Rev. A* **84**, 043832 (2011).
- [45] J. F. Huang and C. K. Law, Photon emission via vacuum-dressed intermediate states under ultrastrong coupling, *Phys. Rev. A* **89**, 033827 (2014).
- [46] A. Ridolfo, M. Leib, S. Savasta, and M. J. Hartmann, Photon blockade in the ultrastrong coupling regime, *Phys. Rev. Lett.* **109**, 193602 (2012).
- [47] C. Groiseau, A. I. Fernández-Domínguez, D. Martín-Cano, and C. Sánchez Muñoz, Single-Photon Source Over the Terahertz Regime, *PRX Quantum* **5**, 010312 (2024).
- [48] T. Niemczyk, F. Deppe, H. Huebl, E. P. Menzel, F. Hocke, M. J. Schwarz, J. J. García-Ripoll, D. Zueco, T. Hümmer, E. Solano, A. Marx, and R. Gross, Circuit quantum electrodynamics in the ultrastrong-coupling regime, *Nat. Phys.* **6**, 772 (2010).
- [49] P. Forn-Díaz, J. Lisenfeld, D. Marcos, J. J. García-Ripoll, E. Solano, C. J. P. M. Harmans, and J. E. Mooij, Observation of the Bloch-Siegert Shift in a Qubit-Oscillator System in the Ultrastrong Coupling Regime, *Phys. Rev. Lett.* **105**, 237001 (2010).
- [50] A. Baust, E. Hoffmann, M. Haerberlein, M. J. Schwarz, P. Eder, J. Goetz, F. Wulschner, E. Xie, L. Zhong, F. Quijandría, D. Zueco, J.-J. García Ripoll, L. García-Álvarez, G. Romero, E. Solano, K. G. Fedorov, E. P. Menzel, F. Deppe, A. Marx, and R. Gross, Ultrastrong coupling in two-resonator circuit QED, *Phys. Rev. B* **93**, 214501 (2016).
- [51] F. Yoshihara, T. Fuse, S. Ashhab, K. Kakuyanagi, S. Saito, and K. Semba, Superconducting qubit-oscillator circuit beyond the ultrastrong-coupling regime, *Nat. Phys.* **13**, 44 (2017).
- [52] A. Bayer, M. Pozimski, S. Schambeck, D. Schuh, R. Huber, D. Bougeard, and C. Lange, Terahertz Light-Matter Interaction beyond Unity Coupling Strength, *Nano Lett.* **17**, 6340 (2017).
- [53] V. M. Muravev, I. V. Andreev, I. V. Kukushkin, S. Schmult, and W. Dietsche, Observation of hybrid plasmon-photon modes in microwave transmission of coplanar microresonators, *Phys. Rev. B* **87**, 045307 (2011).
- [54] G. Scalari, C. Maissen, D. Turćinková, D. Hagenmüller, S. De Liberato, C. Ciuti, C. Reichl, D. Schuh, W. Wegscheider, M. Beck, and J. Faist, Ultrastrong Coupling of the Cyclotron Transition of a 2D Electron Gas to a THz Metamaterial, *Science* **335**, 1323 (2012).
- [55] C. Maissen, G. Scalari, F. Valmorra, M. Beck, J. Faist, S. Cibella, R. Leoni, C. Reichl, C. Charpentier, and W. Wegscheider, Ultrastrong coupling in the near field of complementary split-ring resonators, *Phys. Rev. B* **90**, 205309 (2014).
- [56] T. Schwartz, J. A. Hutchison, C. Genet, and T. W. Ebbesen, Reversible Switching of Ultrastrong Light-Molecule Coupling, *Phys. Rev. Lett.* **106**, 196405 (2011).
- [57] J. George, T. Chervy, A. Shalabney, E. Devaux, H. Hiura, C. Genet, and T. W. Ebbesen, Multiple Rabi Splittings under Ultrastrong Vibrational Coupling, *Phys. Rev. Lett.* **117**, 153601 (2016).
- [58] F. Benz, M. K. Schmidt, A. Dreismann, R. Chikkaraddy, Y. Zhang, A. Demetriadou, C. Carnegie, H. Ohadi, B. D. Nijs, R. Esteban, J. Aizpurua, and J. J. Baumberg, Single-molecule optomechanics in “picocavities”, *Science* **354**, 726 (2016).
- [59] V. Macrì, L. Garziano, A. Ridolfo, O. Di Stefano, and S. Savasta, Deterministic synthesis of mechanical NOON states in ultrastrong optomechanics, *Phys. Rev. A* **94**, 013817 (2016).
- [60] Y. Todorov, A. M. Andrews, R. Colombelli, S. De Liberato, C. Ciuti, P. Klang, G. Strasser, and C. Sirtori, Ultrastrong Light-Matter Coupling Regime with Polariton Dots, *Phys. Rev. Lett.* **105**, 196402 (2010).
- [61] M. Geiser, F. Castellano, G. Scalari, M. Beck, L. Nevou, and J. Faist, Ultrastrong Coupling Regime and Plasmon Polaritons in Parabolic Semiconductor Quantum Wells, *Phys. Rev. Lett.* **108**, 106402 (2012).
- [62] B. Askenazi, A. Vasanelli, Y. Todorov, E. Sakat, J.-J. Greffet, G. Beaudoin, I. Sagnes, and C. Sirtori, Midinfrared Ultrastrong Light-Matter Coupling for THz Thermal Emission, *ACS Photonics* **4**, 2550 (2017).
- [63] J.-F. Huang, J.-Q. Liao, L. Tian, and L.-M. Kuang, Manipulating counter-rotating interactions in the quantum Rabi model via modulation of the transition frequency of the two-level system, *Phys. Rev. A* **96**, 043849 (2017).
- [64] M. Reagor, H. Paik, G. Catelani, L. Sun, C. Axline, E. Holland, I. M. Pop, N. A. Masluk, T. Brecht, L. Frunzio, M. H. Devoret, L. Glazman, and R. J. Schoelkopf, Reaching 10ms single photon lifetimes for superconducting aluminum cavities, *Appl. Phys. Lett.* **102**, 192604 (2013).
- [65] T. Zhang, M. Wu, S. R. Cohen, L. Xin, D. Das, K. K. S. Multani, N. Peard, A.-M. Valente-Feliciano, P. B. Wehlander, A. H. Safavi-Naeini, E. A. Nanni, and M. Schleier-Smith, Optically accessible high-finesse millimeter-wave resonator for cavity quantum electrodynamics with atom arrays, *Phys. Rev. Appl.* **24**, L041001 (2025).
- [66] H. Paik, D. I. Schuster, L. S. Bishop, G. Kirchmair, G. Catelani, A. P. Sears, B. R. Johnson, M. J. Reagor, L. Frunzio, L. I. Glazman, S. M. Girvin, M. H. Devoret, and R. J. Schoelkopf, Observation of High Coherence in Josephson Junction Qubits Measured in a Three-Dimensional Circuit QED Architecture, *Phys. Rev. Lett.* **107**, 240501 (2011).
- [67] T. Charpentier, A. Khvalyuk, L. Ioffe, M. Feigel'man, N. Roch, B. Sacépé, Universal bound on microwave dissipation in superconducting circuits, arXiv:2507.08953.